Microstructure and Mechanical Properties of Si and Sb Added AZ91 Magnesium Alloy

A. SRINIVASAN, U.T.S. PILLAI, and B.C. PAI

The effect of Si (individual and combined) with 0.2 pct Sb additions on the microstructure and mechanical properties of permanent mold AZ91 alloy has been studied. The results indicate that Si addition introduces a Chinese script Mg_2Si phase at the grain boundary along with the $Mg_{17}Al_{12}$ -β phase and reduces ductility and strength of the alloy both at room and high temperatures. A small amount of Sb addition modifies the Mg_2Si phase besides distributing it evenly along the grain boundary. Improved room- and high-temperature mechanical properties are observed in Sb added AZ91 + xSi alloys. However, maximum properties are noticed with the alloy having the combined addition of 0.2 silicon and antimony. Fractograpy of tensile- and impact-tested AZ91 alloy shows cleavage and brittle type of failure. Addition of Si reduces the quasi-cleavage planes, whereas Sb addition increases it while also increasing the plastic zone.

I. INTRODUCTION

MAGNESIUM alloys have been widely used in automobile, aerospace, and electronic industries because of their desirable combination of properties such as low-density high specific strength and specific stiffness, improved damping and electromagnetic shielding capacities, excellent machinability, and good castability.[1,2] These alloys not only offer weight reduction potential when used as structural material in transportation vehicles but also improve the fuel economy and emission regardless of the propulsion system used. During the past decade, the use of magnesium alloy castings in the automobile industry has increased at an impressive rate. AZ91 alloy, which contains 9Al-1Zn-0.2Mn, is the most widely and commercially used Mg alloy system in the automotive industry. Among the Mg alloy components used in transport industries, 90 pct are made from AZ91 alloy.[3] Even though this alloy provides a wide range of room-temperature mechanical properties, it does not exhibit good creep resistance.

To overcome this problem, alloys containing less aluminum Mg-Al-RE (AE) Mg-Al-Si (AS) systems have been developed, and they have exhibited improved high-temperature properties and are used in high-temperature applications.[4] The second phases such as MgRE and Mg_2Si present in AE and AS alloys, respectively, hinder the grain boundary movement and thereby improve the creep properties. However, AS alloys offer only borderline improvement in creep resistance, whereas AE alloys have cost disadvantages due to costly RE addition.[4] Moreover, these alloys are inferior in castability compared to AZ91. Thus, their usage is restricted in high integrity cast components. In the mean time, researchers have started working to develop Mg alloys that provide high creep resistance. Many experimental alloy systems such as Mg-Al-Ca, Mg-Zn-Al-Ca, and Mg-Al-Ca have been developed. However, these alloys are not commercialized so far because of their poor die castability. In the 1990s, work was initiated to modify the microstructure of the AZ91 alloy by introducing thermally-stable intermetallics through addition of alloying elements to improve high-temperature properties.[5]

Surface active elements such as Ca, Bi, and Sb are added to AZ91 alloy to improve creep resistance. Wang *et al.*[6] has investigated the effect of Ca addition into AZ91 alloy and has found that the Ca addition has refined the microstructure and reduced the quantity of $Mg_{17}Al_{12}$ phase by forming a new Al_2Ca phase. The Ca addition has also reduced the ambient temperature properties because of the fact that the Al_2Ca phase has low strength compared to $Mg_{17}Al_{12}$ at room temperature but confers to the elevated temperature strengthening of this alloy. Studies have been carried out on the bismuth addition to AZ91 alloys,[7] which forms a high melting point Mg_3Bi (823 °C) phase, thereby improving the high-temperature properties. Wang *et al.*[8] and Yuan *et al.*[9] studied the effect of Sb addition on the high-temperature properties of AZ91 alloy. The 0.5 pct Sb addition to AZ91 alloy has led to a favorable microstructure by distributing the fine Mg_3Sb particles (melting point around 1228 °C) at the grain boundary and refines the $Mg_{17}Al_{12}$ precipitates, thus improving the room- and high-temperature tensile properties.

It has also been reported[10] that silicon added magnesium alloys (AS41, AS21) have been shown to improve high-temperature properties. A 1 pct silicon addition to die-cast AZ81 alloys improves the mechanical properties and creep resistance, but reduces the ductility. However, reduced mechanical properties are reported in sand or permanent mold castings of Si added Mg alloys, due to the presence of coarse Mg_2Si phase.[4,5,11] Both Ca and P are normally added to refine the Mg_2Si phase in order to obtain improved mechanical properties.

In this study, individual and combined additions of silicon (0.2 and 0.5 pct) and antimony (0.2 pct) have been carried out in AZ91 alloy. Their effects on microstructure, on room-temperature, and on high-temperature mechanical properties have been studied.

II. EXPERIMENTAL

The AZ91 magnesium alloy used for this experiment was prepared by melting together required quantities of commercially

A. SRINIVASAN, Senior Research Fellow, U.T.S. PILLAI, Scientist, and B.C. PAI, Director Grade Scientist, are with the Metal Processing Division, Regional Research Laboratory (CSIR), Trivandrum - 695 019, Kerala State, India. Contact e-mail: utspillai@rediffmail.com or utsubra@yahoo.co.in

Manuscript submitted September 14, 2004.

Table I. Alloy Code and Major Chemical Composition of Alloys

Alloy	Major Compositions					Analyzed Compositions				
	Al	Zn	Mn	Si	Sb	Al	Zn	Mn	Si	Sb
A1	9	1	0.2	—	—	9.3	0.8	0.18	—	—
A2	9	1	0.2	0.2	—	9.5	0.65	0.2	0.22	—
A3	9	1	0.2	0.5	—	8.7	0.72	0.22	0.47	—
A4	9	1	0.2	0.2	0.2	8.3	0.84	0.31	0.26	0.16
A5	9	1	0.2	0.5	0.2	9.3	0.63	0.02	0.52	0.19

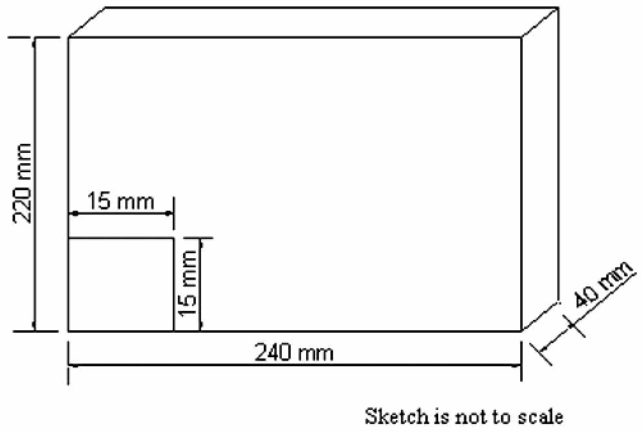

Fig. 1—Schematic diagram showing the casting dimensions and metallography sample location.

available pure Mg, pure Al, pure Zn, and Al-10Mn master alloy. Melting was carried out in a steel crucible in the resistance furnace under proper flux cover. Silicon was added in the form of Al-20Si master alloy and antimony in the form of Al-10Sb master alloy. These additions were carried out when the melt temperature was 700 °C. The melt was refined at 720 °C and then held for 20 minutes for settling oxide particles. The melt was poured into a die-coated metallic mold, which was preheated to 250 °C. Five sets of castings were made with different amounts of Si, with and without Sb addition, to study both the individual and combined addition effects in AZ91 alloy.

The chemical composition analysis of these alloys was carried out using an inductively coupled plasma spectrometer (ICP Plasmascan, model LABTAM 8410). Antimony analysis was carried out by the Gravimetric method. The chemical compositions thus analyzed for the castings are presented in Table I. Microstructural samples drawn from different castings of the same location (as shown in Figure 1) were superficially ground using 4000 grit paper and then polished with 0.25-μm diamond paste subsequently etched by an etchant (solution of 5 mL acetic acid, 10 mL H_2O, 6 g picric acid, and 100 mL ethanol). X-ray diffraction studies were carried out on the alloy containing different alloying elements using a PHILIPS* PW 1710 powder diffractometer with Cu K_α radiation. The composition of Si and Sb bearing phases was examined in a JEOL,* JSE 35C scanning electron microscope (SEM) with an attached energy-dispersive spectroscope (EDS).

*PHILIPS is a trademark of Philips Electronic Instruments, Mahwah, NJ.

*JEOL is a trademark of Japan Electron Optics Ltd., Tokyo.

Tensile specimens in accordance with the ASTM E8 Standard were machined out from the castings and the room- and the high-temperature (150 °C) tensile tests were performed using an Instron universal testing machine (Instron Corp., England) with a crosshead speed of 2 mm/min. The impact specimens of size 10 × 10 × 55 mm^3 having 2-mm depth notch having 9-deg angle were also machined out and used to measure the impact strength of the alloys at ambient temperature using a Charpy impact test machine.

To understand the micromechanism of fracture, the fractured surfaces of the tensile- and impact-tested specimens were cut and cleaned with acetone solution using an ultrasonic vibrator (Instron Corp., England) and examined using an SEM.

III. RESULTS AND DISCUSSION

A. *Microstructure*

Figure 2 shows the typical microstructure of permanent mold cast AZ91 alloy. It consists of α-Mg solid solution containing Al and Zn, and the divorced eutectic consists of massive $Mg_{17}Al_{12}$ phase and supersaturated Mg solid solution.[12] Discontinuous precipitates of $Mg_{17}Al_{12}$ are also observed in the vicinity of massive eutectic. The presence of zinc and comparatively faster cooling in permanent mold produces divorced eutectic.[13,14,15] From SEM observations (Figure 2(b)), it can be further confirmed that the AZ91 alloy consists of two kinds of $Mg_{17}Al_{12}$ particles having the same composition. One is the massive $Mg_{17}Al_{12}$ particles with irregular shape and the other one is the small needlelike laminar particles surrounding the massive particles. Continuous cooling after the eutectic temperature leads to the formation of laminar precipitates from the supersaturated eutectic α-solid solution. The XRD analyses preformed on the AZ91 alloy shown in Figure 3 also confirm that the alloy consists of two phases, viz., α-Mg matrix and β-$Mg_{17}Al_{12}$ phase.

Figure 4 shows the microstructure of Si added AZ91 alloy. When 0.2 pct Si is added to AZ91 alloy, a new Mg_2Si phase appears at the grain boundary in addition to the massive $Mg_{17}Al_{12}$ particles. In 0.5Si added alloy, the only microstructural change observed is the increase in the amount of Mg_2Si precipitates, and the Si bearing phase is well-defined Chinese script (Figure 4(b)). Figure 5 shows the SEM photograph of the alloy A3 focusing the Mg_2Si Chinese script phase. Both the EDX and X-ray analyses also confirm the presence of the Mg_2Si particles, and the morphology is consistent with that reported in the literature.[11] It is further noticed from the microstructure that the addition of Si to AZ91 alloy does not change the quantity as well as the morphology of the

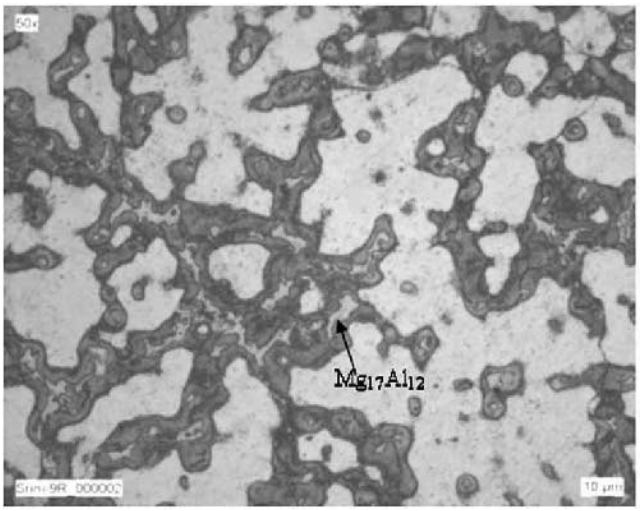

(*a*)

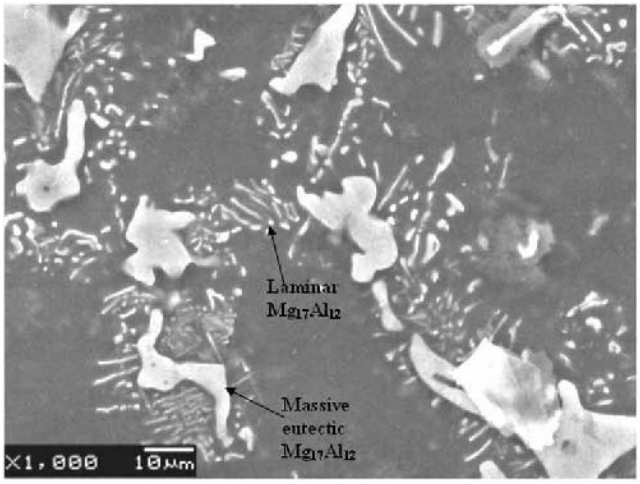

(*b*)

Fig. 2—Microstructure of AZ91 magnesium alloy: (*a*) optical micrograph and (*b*) SEM micrograph showing two kinds of $Mg_{17}Al_{12}$ particles.

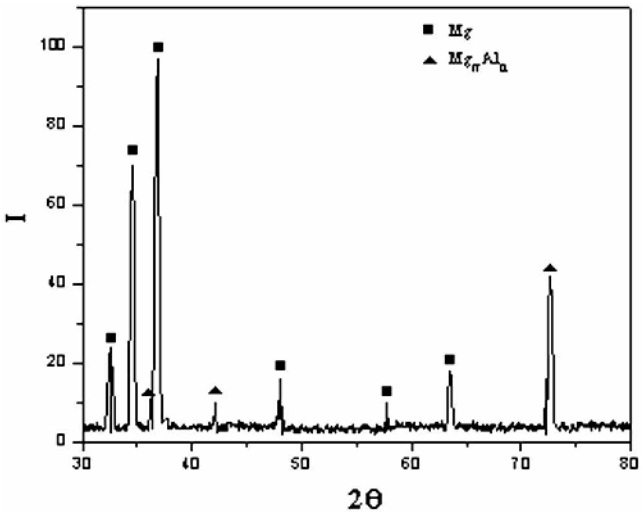

Fig. 3—XRD pattern for the base alloy AZ91.

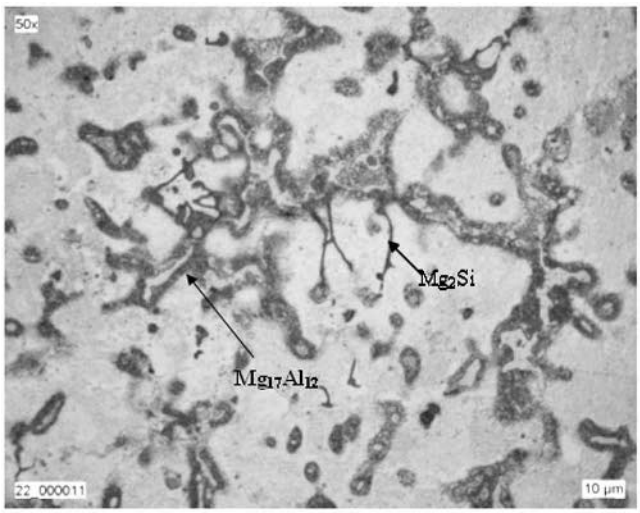

(*a*)

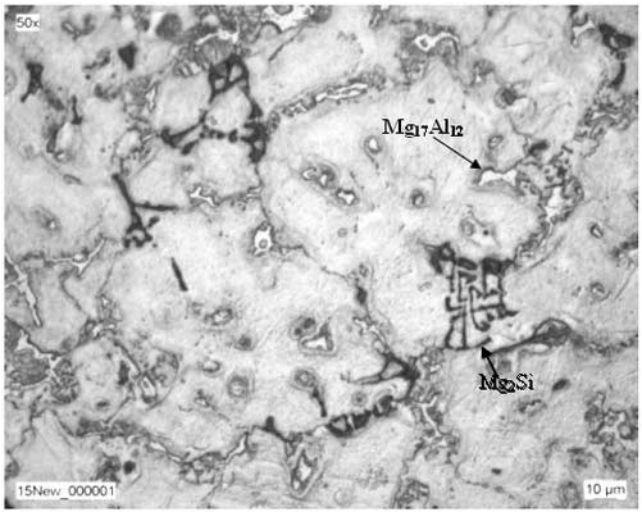

(*b*)

Fig. 4—Microstructure of AZ91 alloy containing Si: (*a*) AZ91 + 0.2Si and (*b*) AZ91 + 0.5Si.

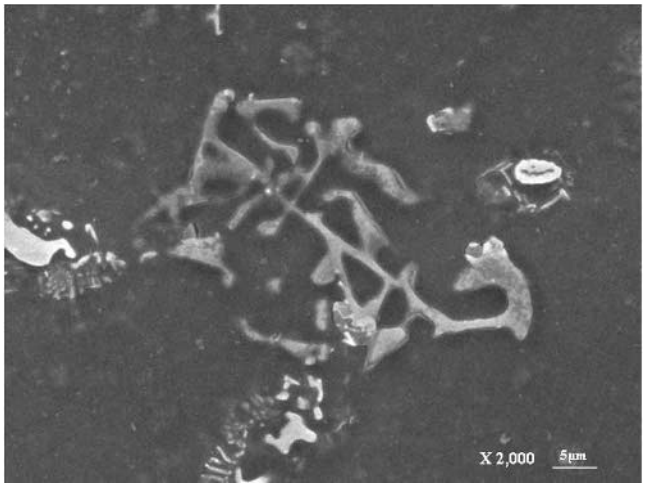

Fig. 5—SEM micrograph showing Chinese script Mg_2Si intermetallics in alloy A3.

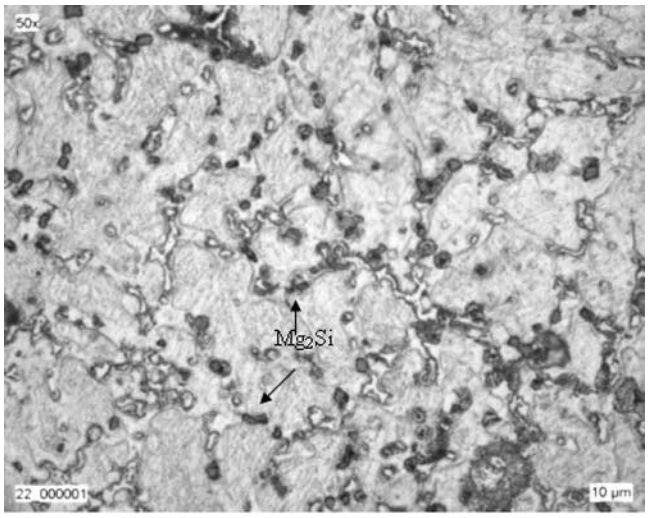

Fig. 6—Micrograph of Sb added AZ91 + 0.5Si alloy showing the refined Mg_2Si particles.

$Mg_{17}Al_{12}$ phase. The quantity is not changed for of two reasons: (1) the possibility of the formation of any other compound containing Al and Si is nil; and (2) the solid solubility of Si in Mg is negligible. The microscopic examination also indicates that the added silicon does not change the morphology of $Mg_{17}Al_{12}$. The EDX analysis performed across the $Mg_{17}Al_{12}$ phases indicates that there is no Si in it. These facts confirm that Si does not act as a refiner or modifier for the $Mg_{17}Al_{12}$ phase.

Figure 6 shows the microstructure of 0.2Sb added AZ91 alloy containing 0.5Si. The addition of 0.2Sb has led to an interesting microstructural change. The massive Chinese script morphology of Mg_2Si precipitates has been changed to a fine polygonal shape besides distributing them evenly along the grain boundaries. Further refinement in the grain size is also noticed in the Sb added alloy. Microstructure of the heat-treated (solutionized at 410 °C for 24 hours subsequently aged at 200 °C for 2 hours) samples shown in Figure 7 confirms the refinement in grain size (~60 μm) in alloy A4 (Figure 7(a)) as compared to the grain size (~80 μm) observed in alloy A1 (Figure 7(b)). The result of the X-ray diffraction pattern of alloy A5 presented in Figure 8 shows the peaks of four phases such as Mg matrix, $Mg_{17}Al_{12}$, Mg_2Si, and Mg_3Sb_2. Even though the presence of Mg_3Sb_2 phases is not clearly seen from the optical micrograph, the secondary electron SEM image and EDX spectrum on the center of the particle confirm the presence of Sb (Figure 9). The Mg_2Si phase contains black particles inside it, which are probably Mg_3Sb_2, which might have acted as a nucleus for Mg_2Si. However, the optimum amount of Sb addition required to refine the Mg_2Si precipitates for different levels of Si is to be studied in detail.

B. *Mechanical Properties*

1. *Tensile properties*

Figure 10 presents the tensile properties of the silicon (with and without Sb addition) added magnesium alloy tested at room temperature. It can be seen from the figure that the Si addition reduces the room-temperature tensile properties compared to the AZ91 base alloy. Reduction in both strength and elongation is observed for Si additions. The presence of coarse Mg_2Si

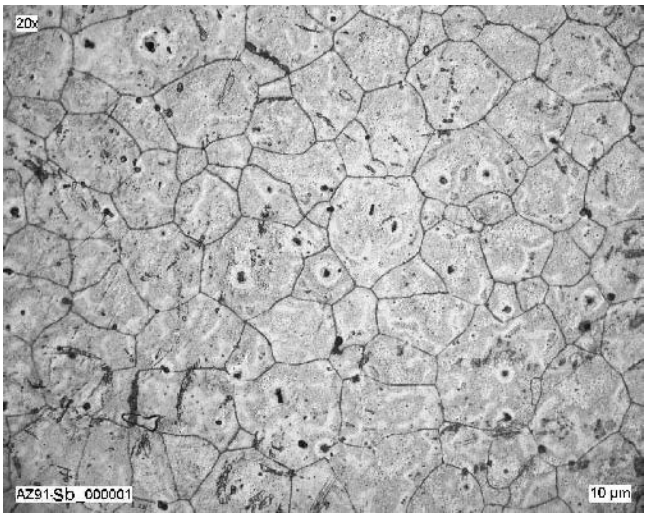

(*a*)

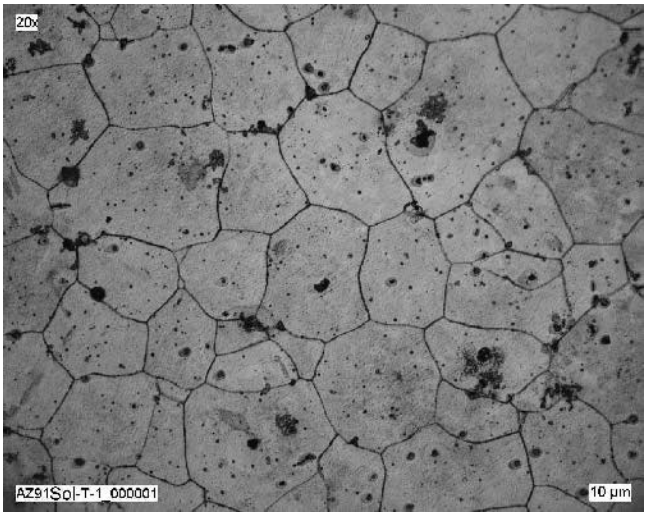

(*b*)

Fig. 7—Heat-treated microstructures showing grain size: (*a*) alloy A4 and (*b*) alloy A1.

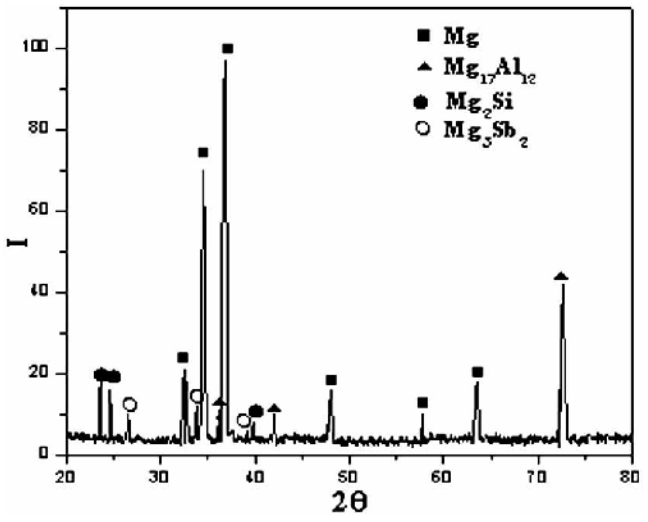

Fig. 8—XRD pattern of alloy A5.

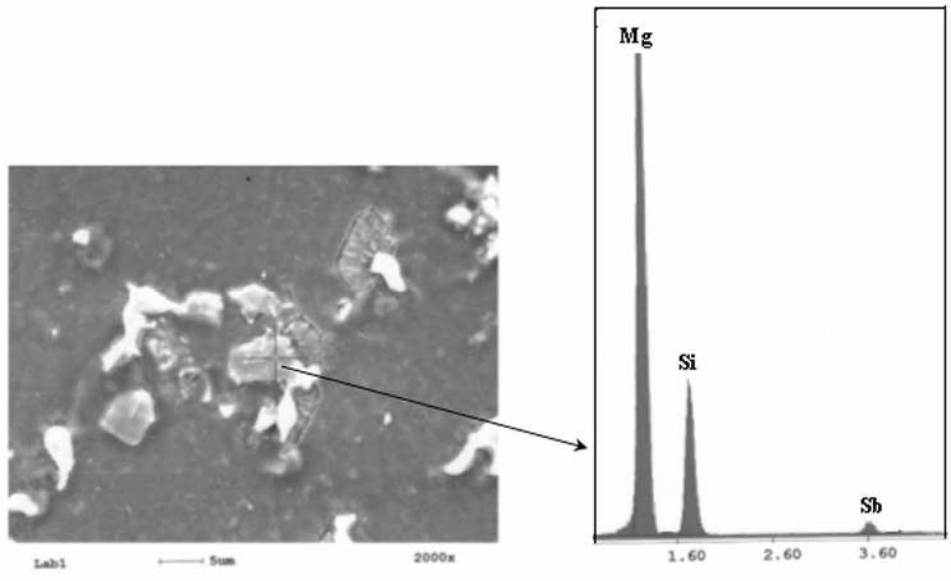

Fig. 9—SEM photograph showing modified Mg_2Si particles and EDS spectrum taken at the center of the particle.

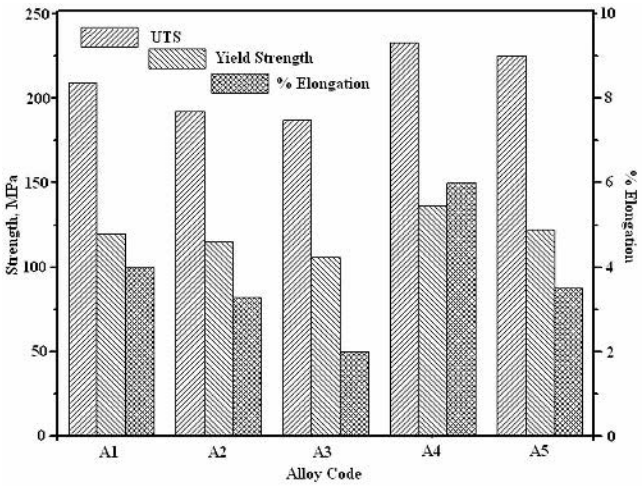

Fig. 10—Tensile properties of the alloys tested at room temperature.

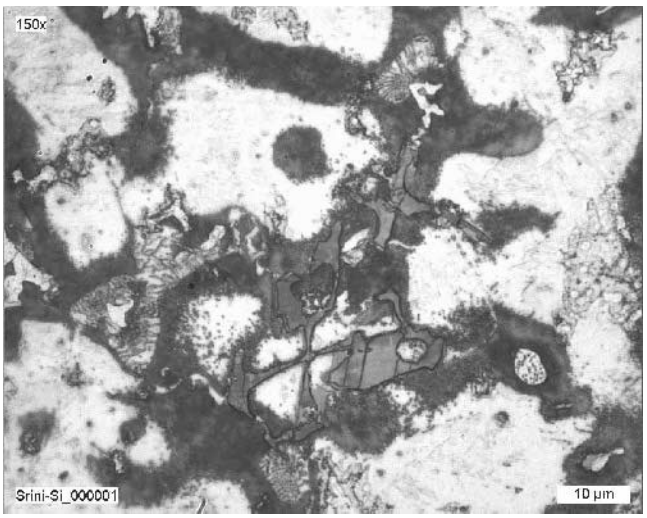

Fig. 11—Optical micrograph showing fractured Mg_2Si particles in alloy A3.

phase in the Si added AZ91 alloys is the reason for reduction in tensile properties; however, more reduction obtained in 0.5Si added alloy is due to the presence of a large amount of coarse Chinese script Mg_2Si precipitates together with the $Mg_{17}Al_{12}$ phase. Normally, in Si containing Mg-Al alloys (AS21 and AS41 alloys), Mg_2Si precipitates out as Chinese script morphology due to slow cooling in the sand and permanent mold castings compared to pressure die casting where the metal solidifies faster. This reduces the mechanical properties, and because of this the AS alloys are restricted to only die castings.[4,5] This is due to the fact that crack will easily nucleate and develop at the interface between the ductile Mg matrix and the coarse Chinese script Mg_2Si precipitates. In the present study also, the number of cracked Mg_2Si particles is confirmed from the micrograph (Figure 11) taken on the cross section just below the tensile fractured surface of the Si added sample. This, along with the weak interface between the α-matrix and the β-$Mg_{17}Al_{12}$ phase, reduces the mechanical properties of the alloy.

The effect of Sb addition on the tensile properties of Si containing AZ91 alloy can be clearly understood from Figure 10. The change in the shape of the Mg_2Si precipitates from the Chinese script to a pentagon shape greatly improves the mechanical properties, particularly the ductility, when 0.2 Sb is added to Si containing AZ91 alloys. The ultimate strength and ductility of 0.2 Sb added AZ91 + 0.2Si alloy increase to 237 MPa and 6 pct, respectively compared to the base alloy value of UTS (209 MPa) and elongation (4 pct). The improvement obtained in strength and ductility with Sb addition is due to the reduction in grain size and refinement in the Mg_2Si phase. Improved strength and ductility are also obtained in A5 alloy compared to A1 (base alloy) and A3 (without Sb) alloys, but it is less than the A4 alloy, which

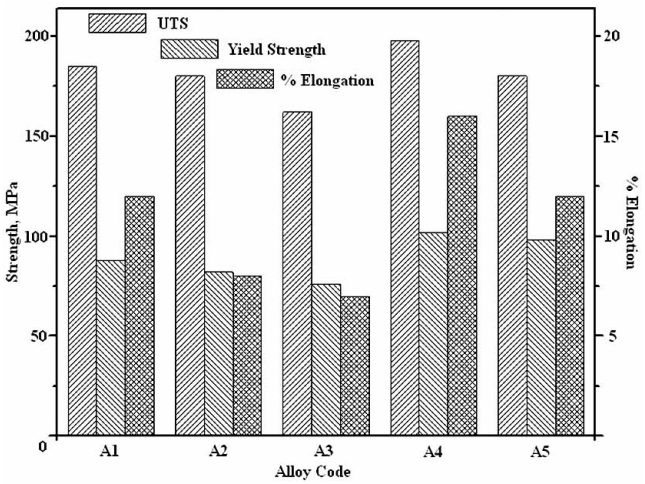

Fig. 12—Tensile properties of the alloys tested at 150 °C.

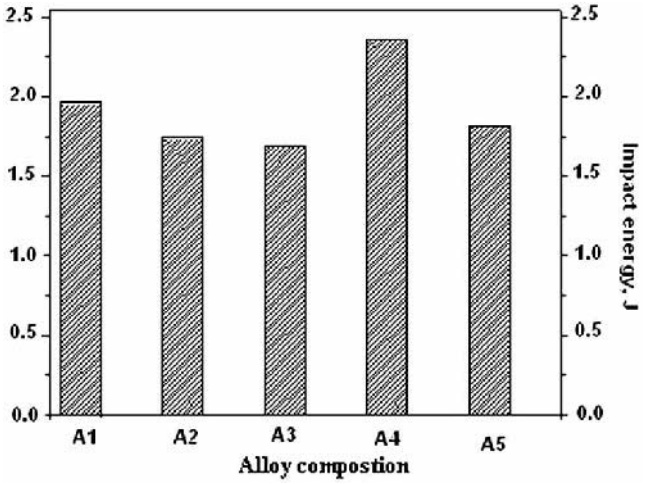

Fig. 13—Effect of Si and Sb addition on impact strength of AZ91 alloy.

clearly indicates that the beneficial effects of Sb are reduced, while the higher amount (0.5 pct) of silicon is added.

The elevated temperature (150 °C) tensile properties of AZ91 alloy containing Si and Sb are shown in Figure 12. It can be observed from the figure that, for all alloys studied, both the UTS and yield strength get decreased in spite of the improvement in ductility noticed at higher testing temperature. In spite of Mg_2Si precipitate's Chinese script morphology, it improves the high-temperature resistance of AZ91 alloy to some extent. The percentage of reduction in strength with Si addition is found to be less, as compared to the base alloy, even though strength (YS and UTS) values obtained are less than that of AZ91 alloy. In A4 and A5 alloys, both the strength and ductility values are found to be higher as compared to the base alloy. This can be explained by the fact that mechanical properties of an alloy consisting of a ductile phase and a hard brittle phase will depend on how the brittle phase is distributed in the microstructure. The condition of optimum strength and ductility is obtained when the brittle phase is present as a fine dispersion uniformly distributed throughout the soft matrix.[16] In the present case, fine and evenly distributed Mg_2Si precipitates due to the addition of a small amount of Sb improve the mechanical properties.

As far as AZ91 alloy is concerned, at room temperature, the main strengthening element is $Mg_{17}Al_{12}$ intermetallics. However, this intermetallic has a low melting point (437 °C) and has a tendency to become coarse at elevated temperature, *i.e.*, above 100 °C, and no longer acts as a barrier for dislocations.[17,18] Moreover $Mg_{17}Al_{12}$ has a cubic crystal structure, which is incoherent with the hcp magnesium matrix.[19] Therefore, this phase leads to the poor elevated temperature properties of AZ91 alloy. Addition of Si to AZ91 alloy forms Mg_2Si precipitate, which has very high melting point (1102 °C) and thermal stability compared to $Mg_{17}Al_{12}$ precipitates, because Si diffuses very slowly in Mg at higher temperatures.[20] Moreover, Mg_2Si precipitates in the refined form with the Sb addition, effectively acts as a dislocation barrier at elevated temperature and pins the grain boundary, hence improving the elevated temperature behavior.

2. *Impact properties*

The impact properties of Si and Sb added to AZ91 alloy are presented in Figure 13. It can be deduced from the figure that the addition of Si reduces the impact properties of the base alloy. However, the Sb added AZ91 + 0.2Si alloy yields higher impact strength than the base AZ91 alloy. It can be further noticed that again for high (0.5 pct) Si added alloy, the impact strength is reduced in spite of Sb addition. This is due to the fact that the impact strength is directly related to the ductility of the alloy, and the presence of a higher amount of coarse, brittle, Chinese script Mg_2Si precipitates due to the addition of 0.5 pct Si to AZ91 alloy reduces the ductility. The change in morphology of Mg_2Si precipitates in A4 alloy due to Sb addition has improved the ductility and hence yields higher impact strength.

It is worth mentioning here that even though the addition of Si and Sb improves the mechanical properties, the effect of these additions on the corrosion properties needs further investigation. However, it is already reported in the literature that addition of Si to Mg-Al alloys does not affect the corrosion properties due to the fact the Mg_2Si precipitates exhibit corrosion potential similar to that of magnesium and hence have a negligible influence on corrosion resistance.[21]

C. *Microfracture Mechanism*

Figure 14(a) shows the fractograph of the tensile fractured surface of AZ91 alloy tested in ambient temperature. In general, the fracture surface reveals cleavage type of failure with some secondary cracks (A in Figure 14(a)). Many cleavage planes (B in Figure 14(a)) with cleavage steps of different sizes and river patterns (C in Figure 14(a)) indicate the brittle failure. The river pattern represents steps between different local cleavage facets of the same general cleavage plane. In AZ91 alloy, the $Mg_{17}Al_{12}$ phases are discontinuously precipitated in coarse lump shape and are very susceptible to fracture because of their brittleness.[22] When load is applied, microcracks are initiated here and they are readily connected to grain boundaries, thereby making the AZ91 alloy brittle. However, in some region, a quasi-cleavage plane (D in Figure 14(a)) with shallow dimples and severe plastic deformation is also seen.

The improvement in ductility in the alloy obtained at 150 °C can be correlated to the fracture surface, which shows greater deformation zone (E in Figure 14(b)); however, the cleavage plane with secondary cracks noticed along

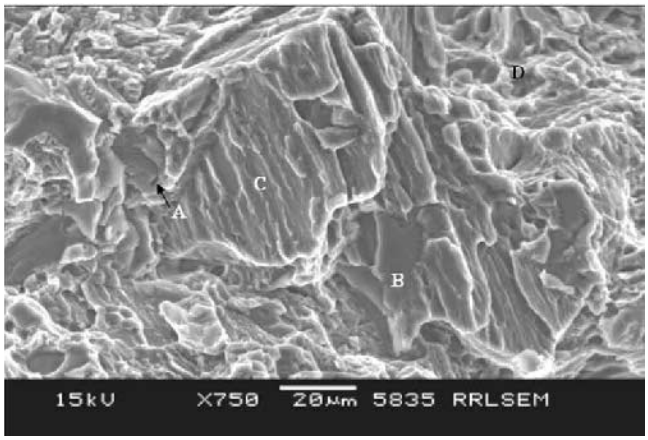

(*a*)

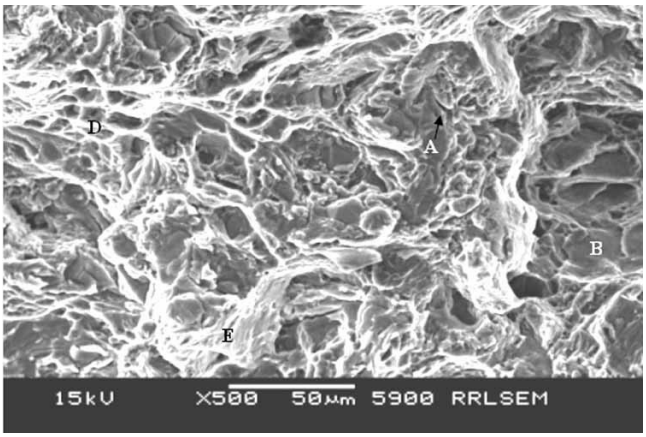

(*b*)

Fig. 14—Tensile fractograph of AZ91 alloy at (*a*) RT and (*b*) 150 °C. (A) secondary crack, (B) cleavage plane, (C) river pattern, (D) quasi-cleavage plane, and (E) plastic deformation.

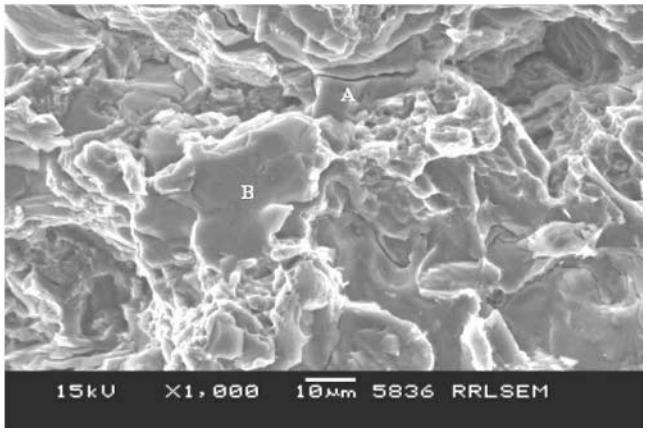

(*a*)

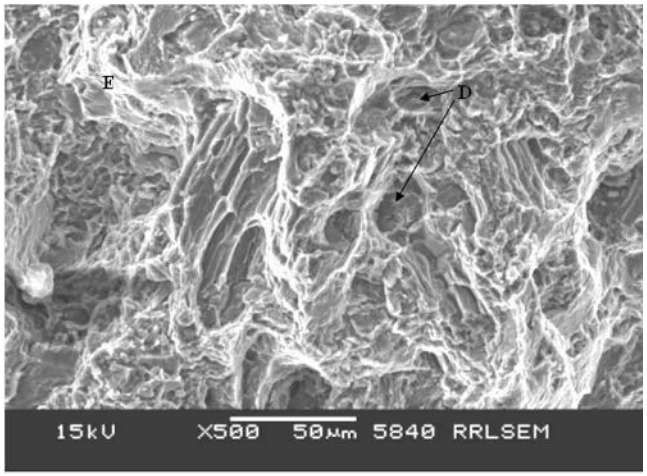

(*b*)

Fig. 15—Tensile fractograph of AZ91 alloy containing (*a*) 0.2 Si and (*b*) 0.2 Si + 0.2Sb. (A) secondary crack, (B) cleavage plane, (D) quasi-cleavage plane, and (E) plastic deformation.

with the deformation zone ensures the brittle fracture (Figure 14(b)). More cleavage facets connected with tearing ridges and shallow dimples ensure the high elongation values obtained at 150 °C temperature. This is likely due to the introduction of additional slip planes such as pyramid and prismatic planes through which cross-slip takes place at elevated temperature.[23]

With 0.2Si addition, well-defined cleavage planes with multiple secondary cracks are observed (Figure 15(a)). Cleavage planes without river pattern observed indicate that the grain may have been orientated at a right angle to the main tensile axis, causing the fracture to propagate very easily on a single plane.[24] While comparing the fracture surface of the base alloy (Figure 14(a)), the plastic zone in the Si added alloy is confined rather than distributed due to the presence of coarse and brittle Mg_2Si particles, which make the alloy more brittle. This is further supported by the number of cracked Mg_2Si particles noticed from the micrograph of the tensile fractured surface of Si added sample (Figure 11).

Addition of Sb changes the fracture mode from cleavage to quasi-cleavage, which is evident from the fracture surface where the presence of a greater number of plastic zones has spread over the entire fracture surface, as seen in Figure 15(b). In quasi-cleavage fracture, the cracks initiate and grow locally and finally form a pitlike morphology on the fracture surface. The bottom of the pits is not made up of strict cleavage planes, but consists of several, albeit somewhat sunken, planes with secondary cracks.[25] Many quasi-cleavage facets connected by tear ridges and shallow dimples ensure the high ductility and strength obtained in this alloy.

Figure 16 shows the fractograpy of impact specimens. When sudden impact load is applied, the stress distribution is nonuniform, which leads to different fracture behavior in different parts of the specimen.[26] This makes the fracture process more complicated. The fracture surface of AZ91 alloy once again exhibits the brittle fracture having cleavage planes with river pattern (Figure 16(a)). More tearing ridges and deformation are seen than the tensile fracture surface. Cleavage tongues (F in Figure 16(a)) are also observed in some cleavage facets, which can be related to mechanical twinning. Tongues are believed to have formed by local fracture along with a twin-matrix interface.[27] These twins are formed as a result of the high rates of deformation in front of the advancing crack.

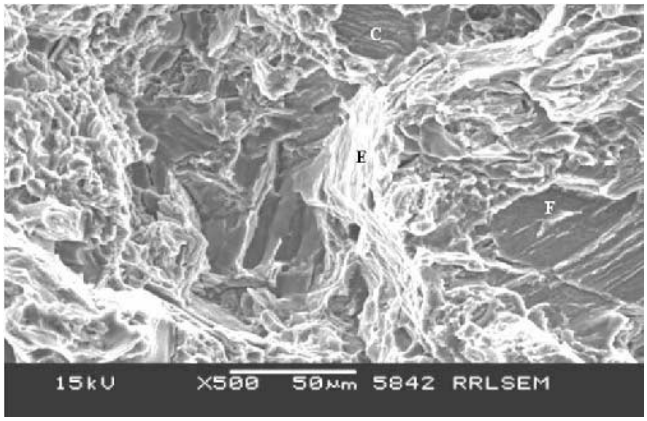

(*a*)

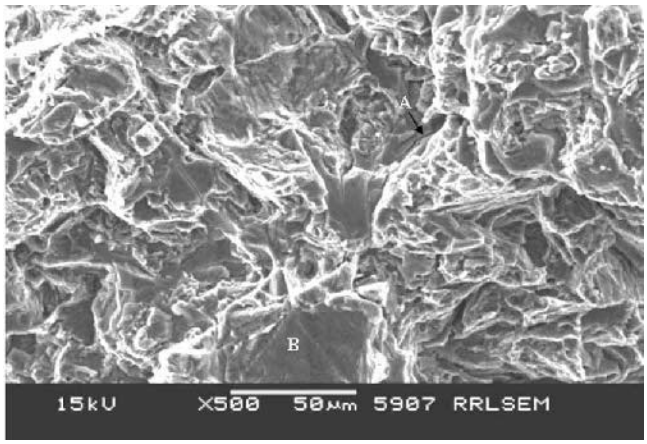

(*b*)

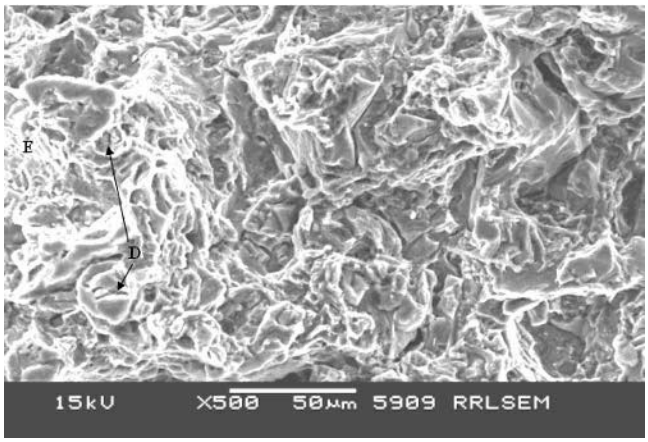

(*c*)

Fig. 16—Fractograph of impact tested specimens: (*a*) AZ91, (*b*) AZ91 + 0.2 Si, and (*c*) AZ91 + 0.2Si + 0.2Sb. (A) secondary crack, (B) cleavage plane, (C) river pattern, (D) quasi-cleavage plane, (E) plastic deformation, and (F) cleavage tongues.

Less tearing zone observed with 0.2Si added alloy surface (Figure 16(b)) as compared to Figure 16(a) can be related to the marginally reduced toughness obtained in the alloy. Since the impact load is applied instantaneously, only little time is available for the microcracks to grow and coalesce. Once the main crack is formed at the rear surface (notch tip side fracture surface), it grows fast and leads to failure. However, some secondary cracks seen on the fracture surface are due to the distribution of the stress.[26] However, more tearing ridges and plastic zones seen in the Sb modified alloy (Figure 16(c)) prove that more energy is observed during deformation, which leads to high impact toughness.

IV. CONCLUSIONS

Silicon addition to AZ91 alloy forms coarse Chinese script Mg_2Si precipitates at the grain boundaries along with $Mg_{17}Al_{12}$. The addition of 0.2Sb to the Si added AZ91 alloy not only modifies the Chinese script Mg_2Si phase to a favorable pentagon shape but also distributes it evenly. Both the room and elevated temperature tensile properties are found to improve with the Sb addition; this overcomes the reduction in tensile properties obtained in Si added AZ91 alloy. The maximum property improvement is noticed with 0.2Si + Sb added AZ91 alloy. The fracture mode is influenced by the Si and Sb additions. The Si addition introduces more cleavage planes, whereas the Sb addition increases the plastic deformation.

REFERENCES

1. B.L. Mordike and T. Ebert: *Mater. Sci. Eng*., 2001, vol. A302, pp. 37-45.
2. H. Friedrich and S. Schumann: *J. Mater. Processing Technol*., 2001, vol. 117, pp. 276-81.
3. Du Wenwen, Sun Yangshan, Min Xuegang, Xue Feng, Zhu Min, and Wu Dengyun: *Mater. Sci. Eng*., 2003, vol. A356, pp. 1-7.
4. M.O. Pekguleryuz: *Mater. Sci. Forum*, 2000, vols. 350–351, pp. 131-40.
5. M.O. Pekguleryuz and M.M. Avedesian: *Proc. Magnesium Alloys and Their Application*, April 1992, B.L. Mordike and F. Hehmann, eds., DGM Informationsgesellschaft mbh., Germany, 1992, pp. 213-20.
6. Wang Qudong, Chen Wenzhou, Zeng Xiaoqin, Lu Yizhen, Ding Wenjiang, Zhu Yaping, and Xu Xiaoping: *J. Mater. Sci*., 2001, vol. 36, pp. 3035-40.
7. Yuan Guangyin, Sun Yangshan, and Ding Wenjiang: *Mater. Sci. Eng*., 2001, vol. A308, pp. 38-44.
8. Qudong Wang, Wenzhou Chen, Wenjiang Ding, Yanping Zhu, and M. Mabuchi: *Metall. Mater. Trans. A*, 2001, vol. 32A, pp. 787-94.
9. Yuan Guangyin, Sun Yangshan, Zhang Weiming: *J. Mater. Sci. Lett*., 1999, vol. 18, pp. 2055-57.
10. S.L. Gouling: *Met. Eng. Q*., 1972, vol. 12, pp. 7-13.
11. Jae Joong Kim, Do Hyang Kim, K.S. Shin, and Nack J. Kim: *Scripta Mater*., 1999, vol. 41 (3), pp. 333-40.
12. M.S. Dargusch, G.L. Dunlop, and K. Pettersen: *Proc. Magnesium Alloys and Their Application*, Wolfsburg, 1998, B.L. Mordike and K.V. Kainer, eds., Warkstoff-Informationsgesellschaft mbh., Frankfurt, Germany, 1998, pp. 277-82.
13. ASM Handbook Committee: *Metallography and Microstructures*, ASM INTERNATIONAL, Metals Park, OH, 1985, pp. 425-34.
14. M.D. Nave, A.K. Dahle, and D.H. St John: *TMS Annual Meeting*, Nashville, TN, Mar. 2000, Howard I. Kaplan, John N. Hryn, and Byron B. Clow, eds., TMS, Warrendale, PA, 2000, pp. 233-42.
15. M.D. Nave, A.K. Dahle, and D.H. St John: *TMS Annual Meeting*, Nashville, TN, Mar. 2000, Howard I. Kaplan, John N. Hryn, and Byron B. Clow, eds., TMS, Warrendale, PA, 2000, pp. 243-50.
16. George E. Dieter: *Mechanical Metallurgy*, 2nd ed., McGraw-Hill Series, McGraw-Hill, New York, NY, 1976, pp. 218-19.
17. I.J. Polmear: *Mater. Sci. Technol*., 1994, vol. 10, p. 1.
18. I.J. Polmear: *Mater. Trans. JIM*, 1996, vol. 37, p. 12.
19. A. Luo and M.O. Perquleryuz: *J. Mater. Sci*., 1994, vol. 29, pp. 5259-71.
20. Y.Z. Lu, Q.D. Wang, X.Q. Zeng, Y.P. Zhu, and W.J. Ding: *Mater. Sci. Eng*., 2001, vol. A301, pp. 255-58.
21. O. Lunder, T.K. Aune, and K. Nisancioglu: *Corrosion*, 1987, vol. 43 (5), pp. 291-95

22. Sunghak Lee, Seung Hyuk Lee, and Do Hyang Kim: *Metall. Mater. Trans. A*, 1988, vol. 29A, pp. 1221-35.
23. Regev, E. Aghoin, A. Rosen, and M. Bamberger: *Mater. Sci. Eng.*, 1998, vol. A252, pp. 6-16.
24. *Metals Handbook*, vol. 9, *Fractography and Atlas of Fractographs*, 8th ed., ASM, Metals Park, OH, 1974, pp. 64-65.
25. Yizhen Lu, Qudong Wang, Xiaoqin Zeng, Wenjiang Ding, Chunquan Zhai, and Yanping Zhu: Mater. Sci. Eng., 2000, vol. A278, pp. 66-76.
26. Y.Z. Lu, Q.D. Wang, W.J. Ding, X.Q. Zeng, and Y.P. Zhu: *Mater. Lett.*, 2000, vol. 44, pp. 265-68.
27. David Broek: *Elementary Engineering Fracture Mechanics*, 4th revised ed., Martinus Nijhoff Publishers, Dordrecht, The Netherlands, 1986, pp. 45-46.